ACS APPLIED MATERIALS & INTERFACES

Research Article

www.acsami.org

Electrochemical and Catalytic Properties of Ni/$BaCe_{0.75}Y_{0.25}O_{3-\delta}$ Anode for Direct Ammonia-Fueled Solid Oxide Fuel Cells

Jun Yang,* Ahmed Fathi Salem Molouk, Takeou Okanishi, Hiroki Muroyama, Toshiaki Matsui, and Koichi Eguchi*

Department of Energy and Hydrocarbon Chemistry, Graduate School of Engineering, Kyoto University, Kyoto 615−8510, Japan

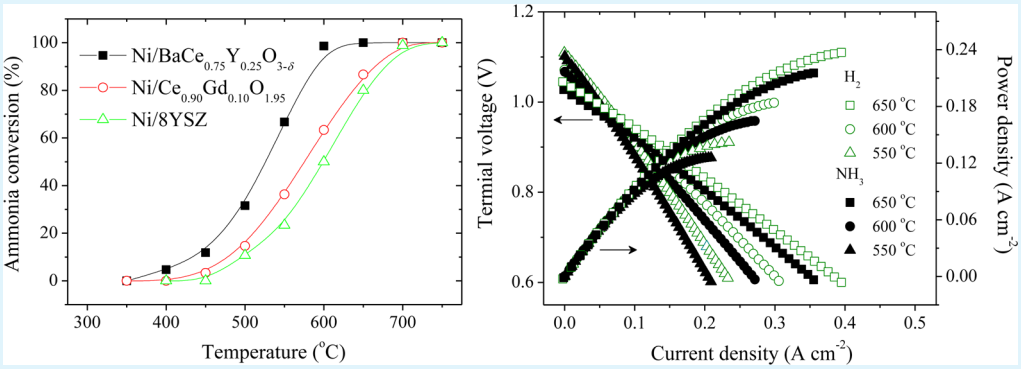

ABSTRACT: In this study, Ni/$BaCe_{0.75}Y_{0.25}O_{3-\delta}$ (Ni/BCY25) was investigated as an anode for direct ammonia-fueled solid oxide fuel cells. The catalytic activity of Ni/BCY25 for ammonia decomposition was found to be remarkably higher than Ni/8 mol % Y_2O_3−ZrO_2 and Ni/$Ce_{0.90}Gd_{0.10}O_{1.95}$. The poisoning effect of water and hydrogen on ammonia decomposition reaction over Ni/BCY25 was evaluated. In addition, an electrolyte-supported SOFC employing $BaCe_{0.90}Y_{0.10}O_{3-\delta}$ (BCY10) electrolyte and Ni/BCY25 anode was fabricated, and its electrochemical performance was investigated at 550−650 °C with supply of ammonia and hydrogen fuel gases. The effect of water content in anode gas on the cell performance was also studied. Based on these results, it was concluded that Ni/BCY25 was a promising anode for direct ammonia-fueled SOFCs. An anode-supported single cell denoted as Ni/BCY25|BCY10|$Sm_{0.5}Sr_{0.5}CoO_{3-\delta}$ was also fabricated, and maximum powder density of 216 and 165 mW cm^{-2} was achieved at 650 and 600 °C, for ammonia fuel, respectively.

KEYWORDS: *ammonia fuel, solid oxide fuel cells, yttrium-doped barium cerate, yttria-stabilized zirconia, gadolinium-doped ceria, proton-conducting oxide, ammonia decomposition*

1. INTRODUCTION

Nowadays, human society is encountering severe environmental and energy crisis due to the excessive consumption of fossil fuels. Since the 1990s, a hydrogen society has been expected to suppress the greenhouse effect caused by CO_2 emission. Various kinds of fuel cells using hydrogen as a fuel have been developed. However, it is much more difficult to liquefy pure hydrogen than other fuel gases due to the low boiling point of −253 °C, leading to technological difficulties in transportation and storage. In view of this, many studies investigated the feasibility of alternative fuel sources including hydrogen, namely hydrogen carrier. Among them, ammonia has received remarkable attention over the past decade.[1]

Ammonia is one of the most produced chemical commodities in this world. It is widely used as fertilizer, refrigerant, and precursor of nitrogenous compounds. As a fuel, ammonia has many advantages such as low cost, high volumetric energy density, and ease in liquefaction (−33 °C at atmospheric pressure or 10 atm at ambient temperature). Ammonia is irritating even at an extremely low concentration in the atmosphere and easy to be sensed even by human's nose, which to some extent lowers the risk of leakage. It is also suggested that the safety issue of ammonia can be avoided by storing ammonia in solid chemicals such as metal amine salts and urea.[1] The use of ammonia fuel in the following "green" energy chain is expected to contribute to reduce CO_2 emission. Hydrogen is produced by carbon−free technologies such as photochemical water splitting and water electrolysis. Electricity needed is generated by renewable energy technologies such as solar cells, wind power, water power stations, etc. Hydrogen is used for ammonia synthesis by the Haber−Bosch process, which is the most matured large−scale ammonia production method. Ammonia can be easily transported to and stored in the destination field because of the mild requirement for liquefaction. Then, ammonia is supplied to energy conversion devices such as fuel cells to generate electricity. In this energy chain, the use of hydrocarbon fuels is significantly suppressed, leading to the reduction of CO_2 emission.[1]

Received: February 8, 2015
Accepted: March 2, 2015
Published: March 2, 2015

DOI: 10.1021/acsami.5b01048
ACS Appl. Mater. Interfaces 2015, 7, 7406−7412

Table 1. Publication List of Fuel Cell Performance Using Ammonia-Containing Fuel

electrolyte	cathode	oxidant	anode	fuel	T (°C)	max power density (mW cm^{-2})	ref
8 mol % Y_2O_3–ZrO_2 (YSZ)	Pt	O_2	Pt	7% NH_3/93% N_2	1000	130	4
YSZ	Ag	air	Ni/YSZ	NH_3	800	60	5
$Ce_{0.8}Sm_{0.2}O_{1.9}$	$Sm_{0.5}Sr_{0.5}CoO_{3-\delta}$/ $Ce_{0.8}Sm_{0.2}O_{1.9}$	O_2	Ni/$Ce_{0.8}Sm_{0.2}O_{1.9}$	NH_3	750	250	6
YSZ	$La_{0.67}Sr_{0.33}MnO_{3+\delta}$/YSZ	air	Ni/YSZ	NH_3	800	200	7
YSZ	YSZ/$La_{0.5}Sr_{0.5}MnO_{3+\delta}$	air	Ni/YSZ	97% NH_3/3% H_2O	750	299	8
$Ce_{0.8}Sm_{0.2}O_{1.9}$	$Ba_{0.5}Sr_{0.5}Co_{0.8}Fe_{0.2}O_{3-\delta}$	air	Ni/$Ce_{0.8}Sm_{0.2}O_{1.9}$	NH_3	650	1190	9
YSZ	$La_{0.6}Sr_{0.4}Co_{0.2}Fe_{0.8}O_{3-\delta}$	air	Ni/YSZ	NH_3	700	400	10
$Sc_{0.1}Zr_{0.9}O_{1.95}$	LSM/YSZ	air	Fe/Ni/YSZ	NH_3	800	1150	11
$La_{0.90}Sr_{0.10}Ga_{0.80}Mg_{0.20}O_{2.85}$	$Sm_{0.5}Sr_{0.5}CoO_{3-\delta}$	air	Fe/$Ce_{0.8}Sm_{0.2}O_{1.9}$	NH_3	900	390	12
$BaCe_{0.80}Gd_{0.19}Pr_{0.01}O_{3-\delta}$	Pt	air	Pt	NH_3	700	35	13
$BaCe_{0.85}Eu_{0.15}O_{3-\delta}$	Pt	air	Pt	NH_3	700	38	14
$BaCe_{0.8}Gd_{0.2}O_{3-\delta}$	$La_{0.5}Sr_{0.5}CoO_{3-\delta}$/ $BaCe_{0.8}Gd_{0.2}O_{3-\delta}$	97% O_2/3% H_2O	Ni/$BaCe_{0.8}Gd_{0.2}O_{3-\delta}$	NH_3	750	380	15
$BaCe_{0.9}Nd_{0.1}O_{3-\delta}$	$La_{0.5}Sr_{0.5}CoO_{3-\delta}$/ $BaCe_{0.9}Nd_{0.1}O_{3-\delta}$	air	Ni/$BaCe_{0.9}Nd_{0.1}O_{3-\delta}$	NH_3	700	315	16
$BaCe_{0.8}Gd_{0.2}O_{3-\delta}$	$Ba_{0.5}Sr_{0.5}Co_{0.8}Fe_{0.2}O_{3-\delta}$/ $Ce_{0.8}Gd_{0.2}O_{1.9}$	O_2	Ni/$Ce_{0.8}Gd_{0.2}O_{1.9}$	NH_3	600	147	17
$BaZr_{0.1}Ce_{0.7}Y_{0.2}O_{3-\delta}$	$Ba_{0.5}Sr_{0.5}Co_{0.8}Fe_{0.2}O_{3-\delta}$	air	Ni/ $BaZr_{0.1}Ce_{0.7}Y_{0.2}O_{3-\delta}$	NH_3	600	190	18

In recent years, a great deal of effort has been made to develop direct ammonia fuel cells. For low-temperature fuel cells such as anion exchange membrane fuel cells and alkaline fuel cells, there is still a long way to go because the poisoning species generated from the electro–oxidation reaction of ammonia on anode prevent continuous power generation.[2,3] On the other hand, solid oxide fuel cells (SOFCs), which are characterized by the high-temperature operation, are considered to be suitable for the conversion of ammonia to electricity. The feasibility of direct ammonia utilization by SOFCs has been frequently studied in the literatures.[4−18] Some of the results are summarized in Table 1. Ammonia was supplied to SOFCs employing oxide ion–conducting electrolytes, and interesting performance was obtained at 700–1000 °C.[4−12] At this high temperature region, most of ammonia was decomposed into hydrogen and nitrogen over the Ni/oxide cermet anode, which catalyzed the cracking reaction efficiently. Therefore, the anode outlet gas was composed of nitrogen, water, and remained hydrogen and ammonia, whereas the concentration of NO_x was negligibly small.[5,11] Thanks to the high operating temperature, the unused ammonia in anode off-gas could be easily removed by catalytic reaction.

Attractive results were also reported for ammonia-fueled proton-conducting SOFCs (H–SOFCs).[13−18] Comparing with yttria-stabilized zirconia (YSZ) and gadolinium-doped ceria (GDC), proton-conductive doped barium cerates possess higher electrical conductivity at reduced temperatures (<600 °C).[19] The doped barium cerates exhibit dominant proton conductivity in a wet atmosphere.[20] In this case, it is possible to avoid the generation of NO_x from ammonia and oxide ion via electrochemical oxidation on anode. Besides, the reaction between doped barium cerates and high-content carbon dioxide is considered to be the fatal problem that prohibits the use of doped barium cerates for hydrocarbon-fueled SOFCs. This problem can be avoided by using ammonia as a carbon-free fuel. As is shown in Table 1, barium cerates doped with Eu, Nd, Gd, and (Zr+Y) in the B-site have been used for direct ammonia-fueled SOFCs. Although the cell performance at reduced temperatures was not as high as conventional SOFCs at this early stage, the promising prospect of ammonia–fueled H–SOFC has been confirmed.

Among various kinds of doped barium cerates, yttrium-doped barium cerates ($Ba(Ce,Y)O_3$, BCY) possess the highest electrical conductivity. As is the case of other doped barium cerates, BCY shows predominant proton conductivity.[20] In our previous work, Ni/$BaCe_{0.75}Y_{0.25}O_{3-\delta}$ (Ni/BCY25) cermet anode exhibited promising electrochemical performance for direct ammonia-fueled SOFCs.[21] In this work, therefore, the catalytic properties of Ni/BCY25 cermet powder for ammonia decomposition in a reactant gas simulating anode atmosphere were investigated in details. Furthermore, the influence of catalytic behavior on the electrochemical performance of Ni/BCY25 anode was also studied. Finally, an anode-supported cell was fabricated and its performance was evaluated.

2. EXPERIMENTAL SECTION

2.1. Sample Preparation. $BaCe_{0.75}Y_{0.25}O_{3-\delta}$ (BCY25) and $BaCe_{0.90}Y_{0.10}O_{3-\delta}$ (BCY10) were prepared from $Ba(NO_3)_2$ (Wako Pure Chemical Industries, Ltd.), $Ce(NO_3)_3{\cdot}6H_2O$ (Wako Pure Chemical Industries, Ltd.), and $Y(NO_3)_3{\cdot}6H_2O$ (Aldrich Inc.) by using a citric acid complex method. $Sm_{0.5}Sr_{0.5}CoO_{3-\delta}$ (SSC) was prepared from samarium, strontium, and cobalt nitrate hexahydrates (Wako Pure Chemical Industries, Ltd.) following the method in ref 22. The formation of each phase was confirmed by X-ray diffraction analysis (XRD, Rigaku, Ultima IV X-ray diffractometer). $Ce_{0.9}Gd_{0.1}O_{1.95}$ (GDC, Shin-etsui Chemical Corp.), 8 mol % Y_2O_3-stabilized zirconia (YSZ, Tosoh Corp.), and NiO (Wako Pure Chemical Industries, Ltd.) were commercial products.

NiO and BCY25 powders were mixed and ground in ethanol overnight and then dried. The mixture was calcined at 1200 °C for 5 h, followed by grinding sufficiently in ethanol. The powders of NiO/GDC and NiO/YSZ were prepared in the same manner as NiO/BCY25. The volumetric content of Ni in the three powder samples after reduction treatment was controlled to be 50%.

2.2. Catalytic Activity Tests. The catalytic activity of Ni/BCY25 powder for ammonia decomposition was measured and compared with that of other SOFC anode materials, namely Ni/GDC and Ni/YSZ. The powders of Ni/BCY25, Ni/YSZ, and Ni/GDC were

DOI: 10.1021/acsami.5b01048
ACS Appl. Mater. Interfaces 2015, 7, 7406–7412

calcined at 1400 °C for 5 h prior to catalyst tests, as was the same thermal history of anode, followed by sufficient grind. Each powder was pressed into a pellet at 30 MPa and then pulverized to 7−11 mesh. 0.3 g of the sample was set in a fixed−bed reactor, and reduced at 700 °C for 2 h in 50% H_2−50% Ar under an atmospheric pressure. Subsequently, the reactant gas was supplied and the outlet gas was introduced to an sulfuric acid aqueous solution trap to eliminate residual ammonia. Then, the total flow rate of outlet gas was measured as a function of time by a film flow meter (VP 3, Horiba STEC Co., Ltd.). Ammonia conversion rate was calculated by assuming that the decomposition of ammonia only produced hydrogen and nitrogen. For comparison, the catalytic activity of Ni/GDC and Ni/YSZ was evaluated in the same way. In addition, the effect of water and hydrogen contents in reactant gas on the catalytic activity of Ni/BCY25 for ammonia decomposition was also investigated in detail. In every activity test, the space velocity of reactant gas was fixed at 14 000 L kg^{-1} h^{-1}.

2.3. Cell Fabrication and Testing. Electrolyte-supported and anode-supported cells (hereafter abbreviated as ESC and ASC) were fabricated and tested. BCY10 was used for the electrolyte because it has much higher proton transference number (1.00, 1.00, 0.95, and 0.94 at 500, 550, 600, and 650 °C, respectively) than BCY25 (1.00, 0.83, 0.75, 0.61, at 500, 550, 600, and 650 °C, respectively).[20] For an ESC, BCY10 powder was uniaxially pressed at 30 MPa into a pellet, and then the resultant pellet was isostatically pressed at 200 MPa and sintered at 1600 °C for 5 h. The thickness, diameter, and relative density of as−sintered BCY10 pellet were ca. 1 mm, 18 mm, and 97%, respectively. As the electrical conductivity of BCY25 is the highest in $BaCe_{1-x}Y_xO_{3-\delta}$ systems, this composition was adopted for the anode. NiO/BCY25 powder was mixed with 10 wt % carbon black and polyethylene glycol (molecular weight 400, Wako Pure Chemical Industries, Ltd.) to form slurry, which was subsequently screen-printed on BCY10 pellet and calcined at 1400 °C for 5 h. Platinum electrode was applied on the opposite side of electrolyte pellet to serve as a cathode. The area of both electrodes was 0.28 cm^2. The configuration of ESC was Ni/BCY25|BCY10|Pt. To fabricate an ASC of Ni/BCY25|BCY10|SSC, we mixed NiO/BCY25 powder with 10 wt % poly(vinyl alcohol) and co-pressed with BCY10 powder to laminate the electrolyte layer at 30 MPa, followed by isostatic-pressing at 200 MPa. The as-prepared disc was sintered at 1350 °C for 5 h. The thickness and diameter of electrolyte were ca. 0.06 mm and 18 mm, respectively. Subsequently, SSC cathode with a diameter of 10 mm was applied to the surface of BCY10 electrolyte by a screen−printing method and calcined at 1100 °C for 5 h.

Both ESC and ASC were sandwiched by alumina tubes and sealed by Pyrex glass rings. Before electrochemical tests, anode was reduced in 15% H_2/85% Ar at 650 °C for 2 h. Humidified ammonia- and hydrogen-containing gaseous mixtures were supplied to the anode, and oxygen was used as an oxidant for the cathode. The composition of hydrogen−containing gas was determined by assuming that ammonia in the ammonia-containing gas decomposed to nitrogen and hydrogen completely. For example, the ammonia-containing gas with a composition of 42.9% NH_3−0.8% H_2O−54.5% is converted to hydrogen-containing gas with a composition of 45.0% H_2−1.0% H_2O−54.0% N_2. The details of anode gas composition for ESC and ASC are explained in the following section. The cathode gas was pure oxygen with a flow rate of 100 mL min^{-1}. For an ESC, current−voltage (I−V) characteristics and impedance spectra under different conditions were measured by the CellTest system (Solartron Analytical, UK, potentiostat/galvanostat 1470E and frequency response analyzer 1455). In addition, the anode off−gas was analyzed by a mass spectrometer (OmniStar GSD 320, Pfeiffer Vacuum AG) in order to monitor the change in gas composition caused by the galvanostatic operation. In the case of ASC, I−V characteristics of the cell fueled with ammonia and hydrogen were recorded at 550−650 °C.

3. RESULTS AND DISCUSSION

The catalytic activity of Ni/BCY25 for ammonia decomposition was compared with Ni/GDC and Ni/YSZ as shown in Figure 1. Diluted ammonia (42.9% NH_3−57.1% Ar; total flow rate: 70 mL min^{-1}) was supplied to the catalyst. For every catalyst, the activity for ammonia decomposition increased significantly with rising temperature. At each temperature, the Ni/BCY25 cermet exhibited the highest activity; a high ammonia conversion rate of 98.6% was obtained at 600 °C.

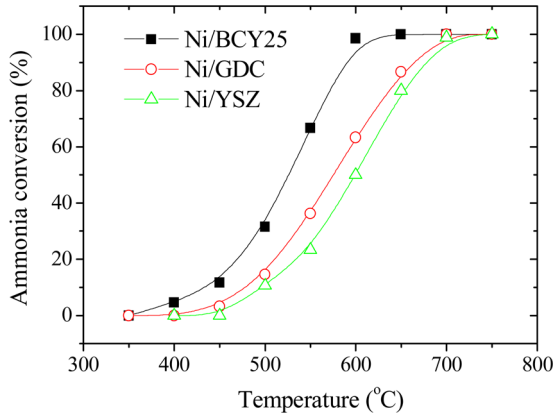

Figure 1. Ammonia conversion over Ni/BCY25, Ni/GDC, and Ni/YSZ with reactant gas of 42.9% NH_3−57.1% Ar; gas space velocity: 14 000 L kg^{-1} h^{-1}.

The anode gas for ammonia-fueled SOFC usually consists of ammonia, water, nitrogen, and hydrogen. It was confirmed in the literature that nitrogen concentration would not affect ammonia decomposition over Ni catalyst but hydrogen has a poisoning effect.[23] On the other hand, the effect of water concentration on the activity for ammonia decomposition has not been investigated yet. In this study, therefore, the influence of hydrogen and water concentrations on the catalytic activity of anode materials was studied.

A number of studies suggested that the presence of hydrogen in the reactant gas exhibited a poisoning effect on ammonia decomposition over Ni and Ru catalysts because hydrogen would occupy the active reaction sites on catalyst surface.[23−26] The reaction rate of ammonia, r_{NH_3}, mL min^{-1}, can be described by the following equation

$$r_{NH_3} = -\frac{dP_{NH_3}}{dt} = kP_{NH_3}{}^{\alpha}P_{H_2}{}^{\beta} \quad (1)$$

where P_{NH_3} and P_{H_2} are partial pressure of ammonia and hydrogen, Pa, respectively. k, α, and β are constants.[23] In this work, the reaction order of hydrogen, β, was used to evaluate the resistance of catalyst to the hydrogen poisoning effect. In order to obtain β, the reactant gas with fixed P_{NH_3} and different P_{H_2} was supplied to Ni/BCY25 and Ni/GDC in order to measure the reaction rate of ammonia was measured as a function of P_{H_2} at 450−550 °C. A similar experiment was carried out on Ni/YSZ at 500−550 °C because of its low catalytic activity.

The P_{H_2} dependence of r_{NH_3} for Ni/BCY25 and Ni/GDC at 450 °C is shown in Figure 2a. With increasing P_{H_2}, the rate, r_{NH_3}, decreased apparently at 450 °C regardless of catalyst. The constant of β for each catalyst was calculated according to eq 1 and plotted as a function of temperature in Figure 2(b). Minus sign indicates that the existence of hydrogen in the reactant gas retards the reaction rate. The β value of Ni/BCY25 was much

DOI: 10.1021/acsami.5b01048
ACS Appl. Mater. Interfaces 2015, 7, 7406−7412

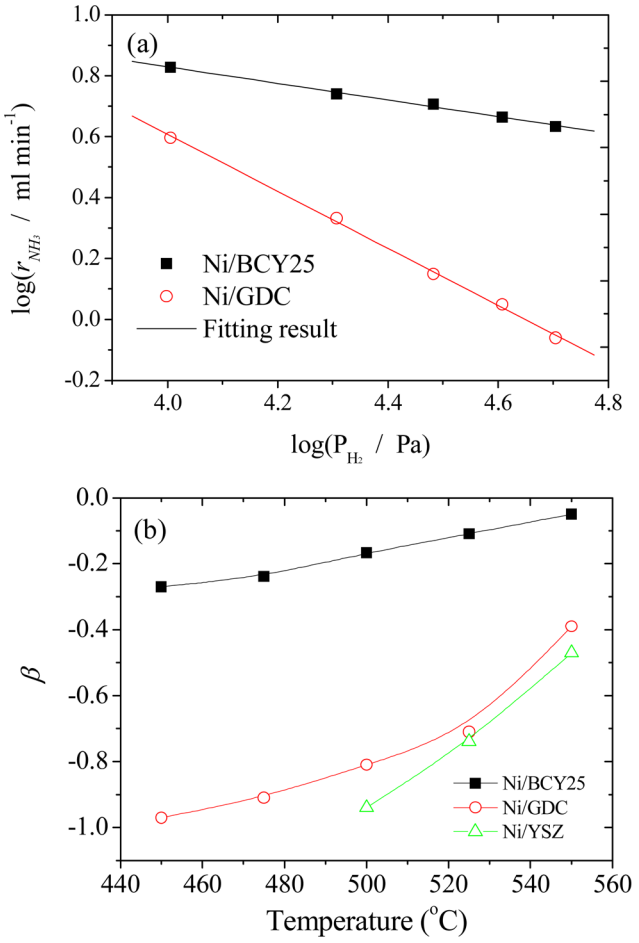

Figure 2. (a) Ammonia reaction rate (r_{NH_3}) for Ni/BCY25 and Ni/GDC as a function of hydrogen partial pressure (P_{H_2}) at 450 °C; (b) β value of Ni/BCY25, Ni/GDC, and Ni/YSZ as a function of temperature; reactant gas: 50.0% NH_3–x% H_2–(50.0–x)% Ar; gas space velocity: 14000 l kg^{-1} h^{-1}.

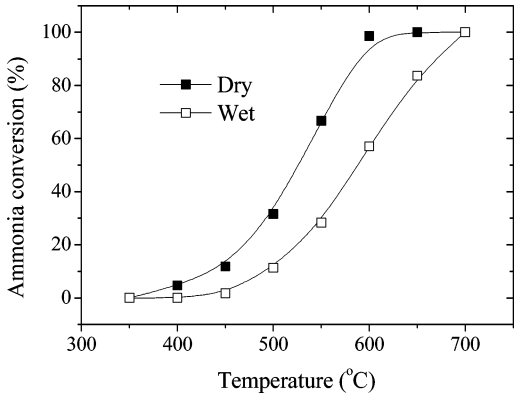

Figure 3. Ammonia conversion over Ni/BCY25 with reactant gases of 42.9% NH_3–57.1% Ar (dry) and 42.9% NH_3–0.8% H_2O–54.5% Ar (wet); gas space velocity: 14 000 L kg^{-1} h^{-1}.

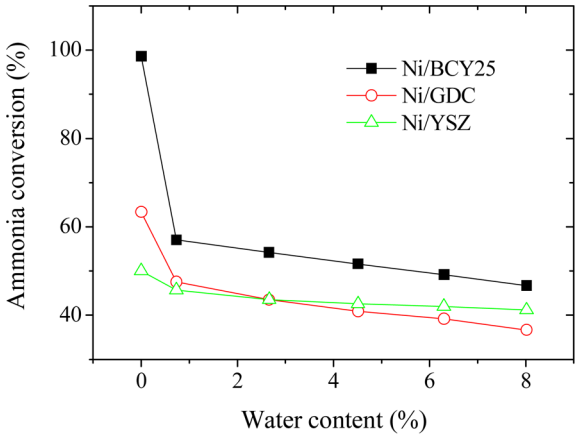

Figure 4. Ammonia conversion over Ni/BCY25, Ni/GDC, and Ni/YSZ as a function of water concentration at 600 °C; reactant gas: 42.9% NH_3–x% H_2O–(57.1–x)% Ar; gas space velocity: 14 000 L kg^{-1} h^{-1}.

closer to zero than Ni/GDC and Ni/YSZ, representing superior resistance to hydrogen poisoning effect. Moreover, Figure 2b shows that the poisoning effect of hydrogen for three catalysts was significantly relieved at higher temperatures, which would be a result of the weaker adsorption of hydrogen on the active reaction sites.

The influence of water content in the reactant gas on ammonia decomposition over Ni/BCY25 is shown in Figure 3. The ammonia conversion over Ni/BCY25 decreased significantly even with an addition of 0.8% water. The poisoning effect of water for Ni/BCY25 was compared with Ni/GDC and Ni/YSZ in Figure 4. The ammonia conversion over Ni/BCY25 at 600 °C dropped sharply from 98.6% to 55.0% when water 0.8% was added and subsequently decreased gradually with increasing water concentration. A similar tendency was observed for Ni/GDC and Ni/YSZ but the extent of drop in ammonia conversion was much smaller. It was reported that the dissociative adsorption of water occurs readily on the surface of BCY25.[27] Thus, the resultant species such as hydroxide group and proton might occupy active reaction sites at the interface between Ni and BCY25, resulting in the strong water poisoning effect.

The influence of catalytic properties of Ni/BCY25 for ammonia decomposition on electrochemical performance was then studied by using the ESC (Ni/BCY25|BCY10|Pt). Ammonia-containing and hydrogen-containing gases were supplied to the Ni/BCY25 anode. Two kinds of anode gases should have the same gas composition if ammonia decomposes to nitrogen and hydrogen completely. Because the BCY10 electrolyte possesses a proton transference number close to unity at the temperature range of 500–650 °C, the influence of oxide ion conduction is negligible in this work. If ammonia is directly converted to electricity, the anode reaction is expressed as follows

$$2NH_3 \rightarrow 6H^+ + N_2 + 6e^- \quad (2)$$

The total reaction in the cell can be written as follows

$$4NH_3 + 3O_2 \rightarrow 2N_2 + 6H_2O \quad (3)$$

The hydrogen generated from ammonia decomposition also serves as the fuel. The reaction is described as

$$H_2 \rightarrow 2H^+ + 2e^- \quad (4)$$

As a result, the total electrochemical reaction is as follows

$$2H_2 + O_2 \rightarrow 2H_2O \quad (5)$$

According to thermodynamics and the Nernst equation, the theoretical open circuit voltages (OCVs) calculated from reaction 3 are much higher than those from reaction 5, as

DOI: 10.1021/acsami.5b01048
ACS Appl. Mater. Interfaces 2015, 7, 7406–7412

can be seen in Figure 5. The experimental OCVs of ESC fueled with two kinds of anode gases were compared with the

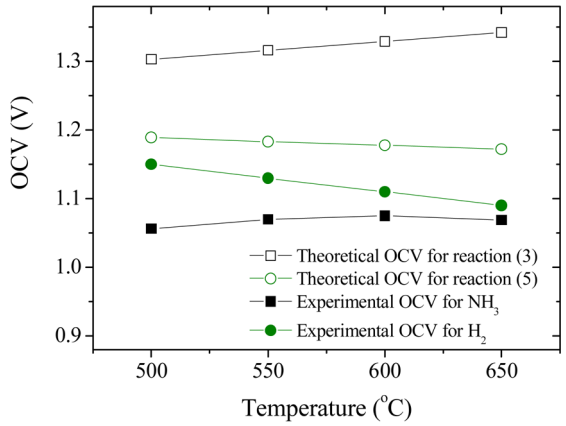

Figure 5. Theoretical and experimental OCVs for ESC (Ni/BCY25|BCY10|Pt) fueled with 45.0% H_2−1.0% H_2O−54.0% N_2 and 42.9% NH_3−1.4% H_2O−55.7% N_2 at 500−700 °C.

theoretical ones. When the anode was exposed to the H_2-containing gas, the OCV was slightly lower than the theoretical one and decreased linearly with a rise in temperature. This tendency agreed well with thermodynamics. The experimental OCV for NH_3-containing anode gas was even lower than that for H_2-containing one. Moreover, the gap between the OCVs for H_2-containing and NH_3-containing anode gases was enlarged apparently at lower temperatures. Analogous tendency was also found for Ni/YSZ and Ni/$Ce_{0.8}Sm_{0.2}O_{1.9}$ anodes in our previous work.[21] It is reasonable to consider that the hydrogen generated from ammonia decomposition served as the main fuel at the anode. The catalytic activity of Ni/BCY25 anode for ammonia decomposition deteriorated at lower temperatures, leading to an increase in the deviation of experimental OCVs for the two kinds of anode gases.

Figure 6 shows *I*−*V* characteristics of the ESC with Ni/BCY25 anode at 550−650 °C. Because the cathode gas composition was fixed, the difference in *I*−*V* curves reflects the response of anode performance to different anode gases. At each temperature, the cell performance was higher in the H_2-

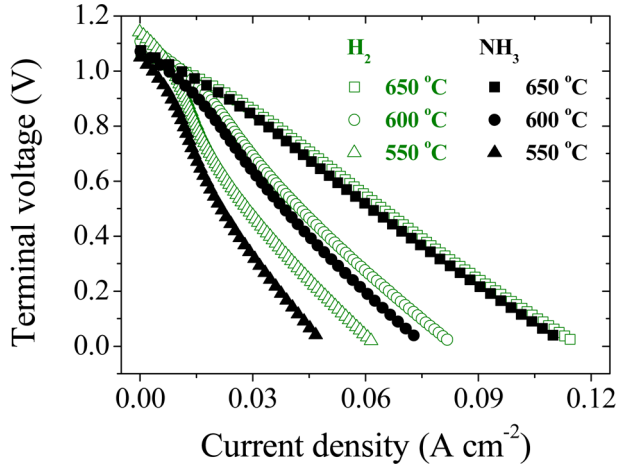

Figure 6. *I*−*V* curves of ESC (Ni/BCY25|BCY10|Pt) fueled with 45.0% H_2−1.0% H_2O−54.0% N_2 and 42.9% NH_3−1.4% H_2O−55.7% N_2; cathode gas: O_2.

containing fuel than in NH_3-containing one. Moreover, the difference in cell performance for the H_2-containing and NH_3−-containing anode gases enlarged apparently with decreasing temperature. The negative effect of temperature decline on catalytic activity of Ni/BCY25 anode for ammonia decomposition was responsible for this phenomenon.

The influence of water content on the cell performance is shown in Figures 7 and 8. As shown in Figure 7, the OCV

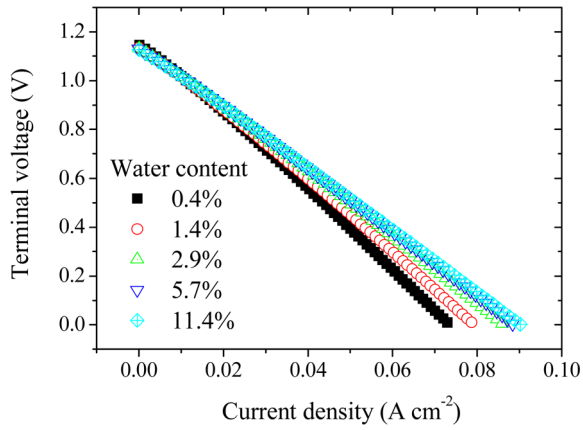

Figure 7. *I*−*V* curves of ESC (Ni/BCY25|BCY10|Pt) fueled with 42.9% NH_3−*x*% H_2O−(57.1−*x*)% Ar (*x*, water content); cathode gas: O_2; temperature: 600 °C.

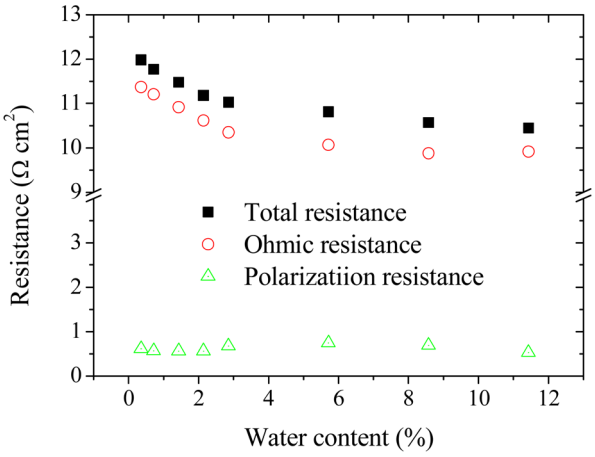

Figure 8. Total, ohmic, and polarization resistances under the open circuit state of ESC: Ni/BCY25|BCY10|Pt fueled with 42.9% NH_3−*x*% H_2O−(57.1−*x*)% Ar (*x*, water content); cathode gas: O_2; temperature: 600 °C.

decreased slightly with increasing water content in anode gas from 0.4 to 2.9% while the current density at low terminal voltage region was apparently raised. However, larger humidity in anode gas did not further improve the cell performance.

Figure 8 shows that with increasing humidity of anode gas, the ohmic resistance, which was dominant for cell performance, was reduced significantly; the polarization resistance was almost stable. As a result, the poisoning effect of water for ammonia decomposition described in Figure 4 did not apparently degrade the cell performance. However, the long−term stability of the anode performance in a humidified atmosphere still needs further investigation, which will be conducted in the near future. The proton conductivity of yttrium-doped barium cerate in the presence of water originates from the incorporation of

DOI: 10.1021/acsami.5b01048
ACS Appl. Mater. Interfaces 2015, 7, 7406−7412

$OH_O^{\bullet}$ (according to Kröger–Vink denotation) at oxygen vacancies ($V_O^{\bullet\bullet}$). The reaction is expressed as follows

$$H_2O + V_O^{\bullet\bullet} + O_O^{\times} \rightarrow 2OH_O^{\bullet} \quad (5a)$$

The resultant proton localized on the lattice oxygen can hop to neighboring oxygen site to exhibit proton conductivity. Increasing humidity raises the concentration of $OH_O^{\bullet}$ and thus elevates the proton conductivity.

After experiments in Figures 7 and 8, the cell was discharged with a supply of ammonia–containing anode gas at current densities of 0.7, 1.1, and 1.4 A cm^{-2} for 600 s, as shown in Figure 9a. The changes of H_2, N_2, and NO_x (NO, NO_2, and N_2O) signals in the anode outlet gas under polarization were monitored by the mass spectrometer. Figure 9b shows that when the discharge started, the mass signal of H_2 decreased rapidly and then kept nearly stable for ca. 400 s. After the interruption of current, the mass signal of H_2 increased to the original level before galvanostatic operation. It is noted that the decrement of H_2 signal during discharge became prominent by increasing current loading. Simultaneously, the mass signal of N_2 increased at the beginning of current loading (see Figure 9c). The increment of N_2 signal indicated the promotion effect of anodic current for ammonia decomposition over Ni/BCY25 anode. This is reasonable because hydrogen is consumed under polarization conditions, which has a poisoning effect for ammonia decomposition as is observed in Figure 2. Throughout this experiment, NO_x (NO, N_2O, and NO_2) species was scarcely detected (<20 ppm). However, considering the ohmic resistance was dominant in this study, the anode polarization was rather small. Therefore, the condition of NO_x formation over anode needs further investigation.

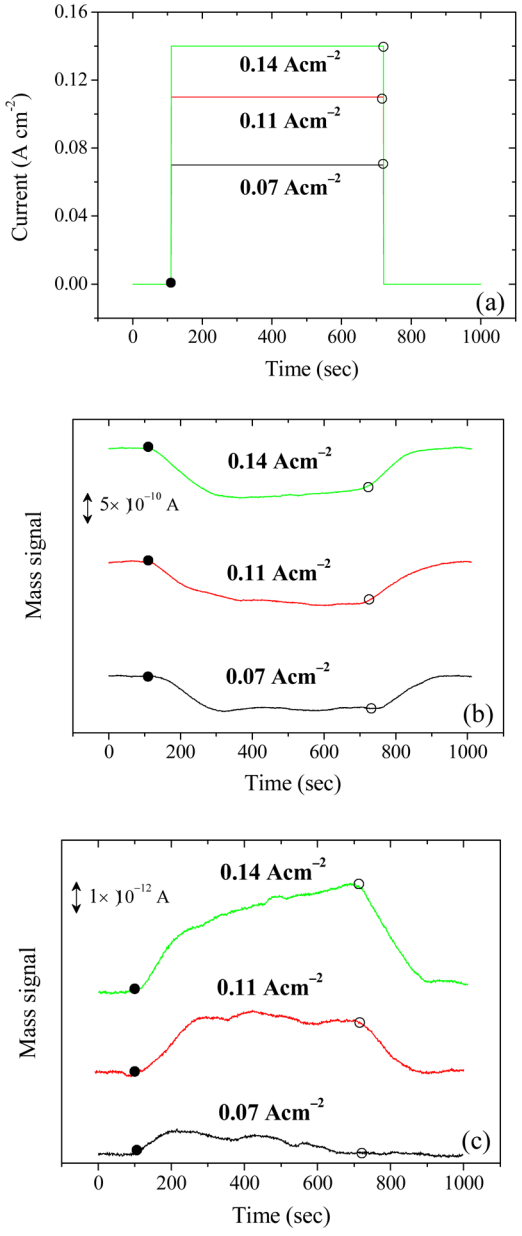

Figure 9. (a) ESC was operated under galvanostatic conditions of 0.07, 0.11, and 0.14 A cm^{-2} at 600 °C, and the mass signals of (b) H_2 and (c) N_2 in the anode off–gas was monitored in response to current loading; solid and open circles represent current on and off, respectively; anode gas: 42.9% NH_3–1.4% H_2O–55.7% N_2; cathode gas: O_2.

An anode-supported cell, ASC (Ni/BCY25|BCY10|SSC), was fabricated. The cell performance at 550–650 °C is shown in Figure 10. At each temperature, the OCV and cell performance under NH_3-fueled conditions was closer to that under H_2-fueled conditions compared with the case of ESC. This is because the ASC is composed of a greater amount of anode catalyst than the ESC, leading to larger gas hourly space velocity. Therefore, ammonia decomposition proceeded sufficiently for ASC. The maximum powder density for ammonia fuel was 216 and 165 mW cm^{-2} at 650 and 600 °C, respectively. It is expected that the cell performance could be further improved by optimizing the fabrication parameters of cell and electrodes such as using thinner electrolyte film.

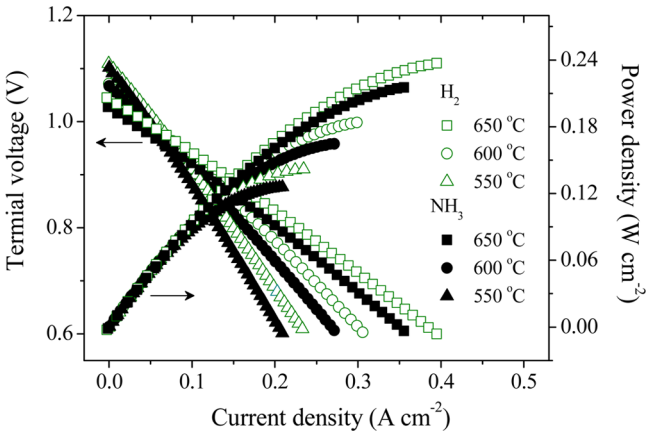

Figure 10. *I–V* curves of ASC at 550–650 °C: Ni/BCY25||BCY10|SSC fueled with 45.0% H_2–1.0% H_2O–54.0% N_2 and 42.9% NH_3–1.4% H_2O–55.7% N_2; cathode gas: O_2.

4. CONCLUSIONS

In this work, the catalytic activity of Ni/BCY25, Ni/GDC, and Ni/YSZ for ammonia decomposition was investigated. It was found that Ni/BCY25 was more active for ammonia decomposition and more resistant to the hydrogen poisoning effect than Ni/GDC and Ni/YSZ. However, ammonia decomposition over Ni/BCY25 was significantly suppressed by water. The electrochemical properties of Ni/BCY25 anode were also investigated with supply of ammonia- and hydrogen-fueled conditions. An anode-supported single cell, Ni/BCY25|

DOI: 10.1021/acsami.5b01048
ACS Appl. Mater. Interfaces 2015, 7, 7406–7412

BCY10|SSC, demonstrated attractive performance was obtained. On the basis of these results, it was concluded that Ni/BCY25 anode possessed excellent electrochemical and catalytic activities, and thus is promising for direct ammonia-fueled SOFCs.

AUTHOR INFORMATION

Corresponding Authors

*E-mail: yangjun03@gmail.com. Phone: +81-75-383-2871. Fax: +81-75-383-2871.

*E-mail: eguchi@scl.kyoto-u.ac.jp. Phone: +81-75-383-2519. Fax: +81-75-383-2520.

Notes

The authors declare no competing financial interest.

ACKNOWLEDGMENTS

This work was supported by Council for Science, Technology and Innovation (CSTI), Cross-ministerial Strategic Innovation Promotion Program (SIP), "energy carrier" (funding agency: JST).

REFERENCES

(1) Rong, L.; Irvine, J.; Tao, S. Ammonia and Related Chemicals as Potential Indirect Hydrogen Storage Materials. *Int. J. Hydrogen Energy* **2012**, *37*, 1482−1494.

(2) Endo, K.; Katayama, Y.; Miura, T. Pt−Ir and Pt−Cu Binary Alloys as the Electrocatalyst for Ammonia Oxidation. *Electrochim. Acta* **2004**, *49*, 1635−1638.

(3) Yang, J.; Muroyama, H.; Matsui, T.; Eguchi, K. Development of a Direct Ammonia-fueled Molten Hydroxide Fuel Cell. *J. Power Sources* **2014**, *245*, 277−282.

(4) Wojcik, A.; Middleton, H.; Damopoulos, I.; Van herle, J. Ammonia as a Fuel in Solid Oxide Fuel Cells. *J. Power Sources* **2003**, *118*, 342−348.

(5) Fournier, G.; Cumming, I.; Hellgardt, K. High Performance Direct Ammonia Solid Oxide Fuel Cell. *J. Power Sources* **2006**, *162*, 198−206.

(6) Ma, Q.; Peng, R.; Tian, L.; Meng, G. Direct Utilization of Ammonia in Intermediate-temperature Solid Oxide Fuel Cells. *Electrochem Commun.* **2006**, *8*, 1791−1795.

(7) Zhang, L.; Cong, Y.; Yang, W.; Lin, L. A Direct Ammonia Tubular Solid Oxide Fuel Cell Chinese. *J.Catal.* **2007**, *28*, 749−751.

(8) Ma, Q.; Ma, J.; Zhou, S.; Yan, R.; Gao, J.; Meng, G. A High-performance Ammonia-fueled SOFC Based on a YSZ Thin-film Electrolyte. *J. Power Sources* **2007**, *164*, 86−89.

(9) Meng, G.; Jiang, C.; Ma, J.; Ma, Q.; Liu, X. Comparative Study on the Performance of a SDC-based SOFC Fueled by Ammonia and Hydrogen J. *Power Sources* **2007**, *173*, 189−193.

(10) Dekker, N.; Rietveld, G. Highly Efficient Conversion of Ammonia in Electricity by Solid Oxide Fuel Cells. *J. Fuel Cell Sci. Technol.* **2006**, *3*, 499−502.

(11) Liu, L.; Sun, K.; Wu, X.; Li, X.; Zhang, M.; Zhang, N.; Zhou, X. Improved Performance of Ammonia-fueled Solid Oxide Fuel Cell with SSZ Thin Film Electrolyte and Ni-SSZ Anode Functional Layer. *Int. J. Hydrogen Energy* **2012**, *37*, 10857−10865.

(12) Akimoto, W.; Fujimoto, T.; Saito, M.; Inaba, M.; Yoshida, H.; Inagaki, T. Ni−Fe/Sm-Doped CeO_2 Anode for Ammonia-Fueled Solid Oxide Fuel Cells. *Solid State Ionics* **2014**, *256*, 1−4.

(13) Pelletier, L.; McFarlan, A.; Maffei, N. Ammonia Fuel Cell Using Doped Barium Cerate Proton Conducting Solid Electrolytes J. *Power Sources* **2005**, *145*, 262−265.

(14) Maffei, N.; Pelletier, L.; Charland, J.; McFarlan, A. An Ammonia Fuel Cell Using a Mixed Ionic and Electronic Conducting Electrolyte J. *Power Sources* **2006**, *162*, 165−167.

(15) Ma, Q.; Peng, R.; Lin, Y.; Gao, J.; Meng, G. A High-Performance Ammonia-Fueled Solid Oxide Fuel Cell. *J. Power Sources* **2006**, *161*, 95−98.

(16) Xie, K.; Ma, Q.; Lin, B.; Jiang, Y.; Guo, J.; Liu, X.; Meng, G. An Ammonia Fuelled SOFC with a $BaCe_{0.9}Nd_{0.1}O_{3-\delta}$ Thin Electrolyte Prepared with a Suspension Spray J. *Power Sources* **2007**, *170*, 38−41.

(17) Zhang, L.; Yang, W. Direct Ammonia Solid Oxide Fuel Cell Based on Thin Proton-conducting Electrolyte J. *Power Sources* **2008**, *179*, 92−95.

(18) Lin, Y.; Ran, R.; Guo, Y.; Zhou, W.; Cai, R.; Wang, J.; Shao, Z. Proton-conducting Fuel Cells Operating on Hydrogen, Ammonia and Hydrazine at Intermediate Temperatures Int. *J. Hydrogen Energy* **2010**, *35*, 2637−2642.

(19) Hibino, T.; Hashimoto, A.; Suzuki, M.; Sano, M. Proton Conduction at the Surface of Y-doped $BaCeO_3$. *J. Phys. Chem. B* **2001**, *105*, 11399−11401.

(20) Suksamai, W.; Metcalfe, I. Measurement of Proton and Oxide Ion Fluxes in a Working Y-doped $BaCeO_3$ SOFC. *Solid State Ionics* **2007**, *178*, 627−634.

(21) Yang, J.; Akagi, T.; Okanishi, T.; Muroyama, H.; Matsui, T.; Eguchi, K. Catalytic Influence of Oxide Component in Ni-based Cermet Anodes for Ammonia-Fueled Solid Oxide Fuel Cells. *Fuel Cells* **2015**, DOI: 10.1002/fuce.201400135.

(22) Koyama, M.; Wen, C.; Masuyama, T.; Otomo, J.; Fukunag, H.; Yamada, K.; Eguchi, K.; Takahashi, H. The Mechanism of Porous $Sm_{0.5}Sr_{0.5}CoO_3$ Cathodes Used in Solid Oxide Fuel Cells. *J. Electrochem. Soc.* **2001**, *148*, A795−A801.

(23) Zhang, J.; Xu, H.; Li, W. Kinetic Study of NH_3 Decomposition over Ni Nanoparticles: the Role of La Promoter, Structure Sensitivity and Compensation Effect Appl. *Catal. A* **2005**, *296*, 257−267.

(24) Yin, S.; Xu, B.; Zhou, X.; Au, C. A Mini-review on Ammonia Decomposition Catalysts for On-site Generation of Hydrogen for Fuel Cell Applications Appl. *Catal. A* **2004**, *277*, 1−9.

(25) Hayashi, F.; Toda, Y.; Kanie, Y.; Kitano, M.; Inoue, Y.; Yokoyama, T.; Hara, M.; Hosono, H. Ammonia Decomposition by Ruthenium Nanoparticles Loaded on Inorganic Electride C12A7:e− Chem. *Sci.* **2013**, *4*, 3124−3130.

(26) Bradford, M.; Fanning, P.; Vannice, M. Kinetics of NH_3 Decomposition over Well Dispersed Ru. *J. Catal.* **1997**, *172*, 479−484.

(27) Kruth, A.; Irvine, J. Water Incorporation Studies on Doped Barium Cerate Perovskites. *Solid State Ionics* **2003**, *162−163*, 83−91.

DOI: 10.1021/acsami.5b01048
ACS Appl. Mater. Interfaces 2015, 7, 7406−7412